JARO: 417–431 (2016)
DOI: 10.1007/s10162-016-0578-4

JARO
Journal of the Association for Research in Otolaryngology

Research Article

Genome-Wide Association Analysis Identifies *Dcc* as an Essential Factor in the Innervation of the Peripheral Vestibular System in Inbred Mice

Pezhman Salehi,[1] Anthony Myint,[1] Young J. Kim,[2] Marshall X. Ge,[1] Joel Lavinsky,[1,3] Maria K. Ho,[1,4] Amanda L. Crow,[5] Charlene Cruz,[1] Maya Monges-Hernadez,[1] Juemei Wang,[1] Jaana Hartiala,[5] Li I. Zhang,[2] Hooman Allayee,[5] Aldons J. Lusis,[5,6] Takahiro Ohyama,[1] and Rick A. Friedman[1,7]

[1]*USC Tina and Rick Caruso Department of Otolaryngology-Head & Neck Surgery, Zilkha Neurogenetic Institute, Keck Medicine of USC, University of Southern California, Los Angeles, CA, USA*

[2]*Department of Physiology and Biophysics, Zilkha Neurogenetic Institute, USC Keck School of Medicine, University of Southern California, Los Angeles, CA, USA*

[3]*Graduate Program in Surgical Sciences, Federal University of Rio Grande do Sul, Porto Alegre, Rio Grande do Sul, Brazil*

[4]*Department of Internal Medicine, Charles E. Schmidt College of Medicine, Florida Atlantic University, Boca Raton, FL, USA*

[5]*Department of Preventive Medicine and Institute for Genetic Medicine, USC Keck School of Medicine, University of Southern California, Los Angeles, CA, USA*

[6]*Department of Microbiology, Immunology, and Molecular Genetics, University of California, Los Angeles, Los Angeles, CA, USA*

Received: 7 March 2016; Accepted: 12 July 2016; Online publication: 18 August 2016

ABSTRACT

This study aimed to investigate the genetic causes of vestibular dysfunction. We used vestibular sensory-evoked potentials (VsEPs) to characterize the vestibular function of 35 inbred mouse strains selected from the Hybrid Mouse Diversity Panel and demonstrated strain-dependent phenotypic variation in vestibular function. Using these phenotypic data, we performed the first genome-wide association study controlling for population structure that has revealed two highly suggestive loci, one of which lies within a haplotype block containing five genes (*Stard6*, *4930503L19Rik*, *Poli*, *Mbd2*, *Dcc*) on Chr. 18 (peak SNP rs29632020), one gene, deleted in colorectal carcinoma (*Dcc*) has a well-established role in nervous system development. An in-depth analysis of *Dcc*-deficient mice demonstrated elevation in mean VsEP threshold for $Dcc^{+/-}$ mice (–11.86 dB) compared to wild-type (–9.68 dB) littermates. Synaptic ribbon studies revealed $Dcc^{-/-}$ (P0) and $Dcc^{+/-}$ (6-week-old) mice showed lower density of the presynaptic marker (CtBP2) as compared to wild-type controls. Vestibular ganglion cell counts of $Dcc^{-/-}$ (P0) was lower than controls. Whole-mount preparations showed abnormal innervation of the utricle, saccule, and crista ampullaris at E14.5, E16.5, and E18.5. Postnatal studies were limited by the perinatal lethality in $Dcc^{-/-}$ mice. Expression analyses using in situ hybridization and immunohistochemistry showed Dcc expression in the mouse vestibular ganglion (E15.5), and utricle and crista ampullaris (6-week-old), respectively. In summary, we report the first GWAS for vestibular functional variation in inbred mice and

Present address: Rick A. Friedman, Department of Otolaryngology, Zilkha Neurogenetic Institute, Keck School of Medicine, University of Southern California, Los Angeles, CA, USA.
Pezhman Salehi, Anthony Myint, and Young J. Kim contributed equally to this work. email: rick.friedman@med.usc.edu

Correspondence to: Takahiro A. Ohyama · USC Tina and Rick Caruso Department of Otolaryngology-Head & Neck Surgery, Zilkha Neurogenetic Institute, Keck Medicine of USC · University of Southern California · Los Angeles, CA, USA. email: takahiro.ohyama@med.usc.edu

provide evidence for the role of *Dcc* in the normal innervation of the peripheral vestibular system.

Keywords: genome-wide association study, vestibular system, Hybrid Mouse Diversity Panel, deleted in colorectal carcinoma (*Dcc*), axonal migration, vestibular sensory evoked potential, utricle, crista, vestibular ganglia

INTRODUCTION

Complaints of dizziness or disequilibrium are common in the elderly, with an estimated lifetime prevalence of 35 % in people over age 60 (Neuhauser et al. 2005). In a recent survey of emergency room visits over a 10-year interval, 26 million visits were recorded for dizziness with an average of over three diagnostic tests per patient, including imaging of the brain in 17 % (Kerber et al. 2008). Unsteadiness is particularly dangerous in the elderly due to increased fall risk.

Dizziness arises from dysfunction of the vestibular system, an elegant and highly conserved neuroanatomical pathway that mediates our ability to perceive angular head motion and linear acceleration. While the etiology of vestibular dysfunction is believed to be multifactorial, there is clear evidence supporting the role of genes in this disease process. A classic example is the family of Usher syndromes, which is a heterogeneous group of genetic disorders characterized by retinal degeneration, deafness, and varying degrees of vertigo depending on the causal gene (Jen 2008). Implicated genes include but are not limited to myosin7a (*MYO7A*), harmonin (*USH1C*), cadherin 23 (*CDH23*), or *PCDH15* (Eppsteiner and Smith 2011; Jones and Jones 2014). Peripheral vestibular dysfunction has also been reported in studies investigating the function of *CLRN1*, *COCH*, *NOX3*, *OTOP1*, *CYBA*, *PLDN* (*BLOC1S6*), *PTPRQ*, *OTOF*, *Kcna10*, and *SLC4A11* genes (Goodyear et al. 2012; Huang et al. 1999; Hurle et al. 2003; Isosomppi et al. 2009; Jones and Jones 2014; Jones et al. 2011; Lee et al. 2013; Nakano et al. 2008; Paffenholz et al. 2004; Vincent et al. 2014).

A genetic basis for vestibular function has also been observed in animals, as different inbred strains of mice exhibit variation in peripheral vestibular function (Jones et al. 2005; Jones et al. 2006). Mouse models have proven instrumental in the identification of genes important for the structural integrity of otoconia, stereocilia, hair cells, inner ear pigment, and the vestibular ganglion. However, no genetic cause for isolated, nonsyndromic peripheral vestibulopathy has been identified (Jones and Jones 2014). A possible explanation presented by the common disease/common variant hypothesis states that common diseases have different underlying genetic architecture than rare disorders (Bush and Moore 2012). Namely, common diseases have multiple susceptibility alleles present in the form of common genetic variation; each susceptibility allele has a relatively small penetrance that only slightly increases risk for disease. However, the combined effect of multiple risk-enhancing alleles with environmental factors ultimately gives rise to disease. This difference in genetic architecture may explain the limited success of traditional genetic mapping methods such as linkage analysis in elucidating the nature of vestibular genetics.

Genome-wide association studies (GWAS) are well suited for the analysis of complex traits. Given the proven utility of the mouse as a model for vestibular function as well as recent advances in mouse genome sequencing and high-density single nucleotide polymorphism (SNP) maps, mice present a convenient platform for GWAS of vestibular function. In this study, we used a GWAS strategy incorporating the Hybrid Mouse Diversity Panel (HMDP) which is a collection of classical inbred (CI) and recombinant inbred (RI) strains whose genomes have been sequenced and/or genotyped at high resolution (Bennett et al. 2010). The resolution obtained using association analyses on this panel is improved by 1–2 orders of magnitude as compared to traditional linkage analysis. Furthermore, power calculations indicate that GWAS with the panel are capable of detecting loci responsible for as little as 5 % of the overall variance. Several studies have successfully mapped candidate loci for complex traits using this panel, and we have published a meta-analysis for age-related hearing loss and strain variation in hearing using the HMDP (Davis et al. 2013; Farber et al. 2011; Hui et al. 2015; Ohmen et al. 2014; Park et al. 2011; Smolock et al. 2012; Zhou et al. 2015).

In this manuscript, we describe the first application of GWAS with correction for population structure to the study of vestibular function in inbred strains of mice. A preliminary screen of vestibular sensory-evoked potential (VsEP) in the HMDP revealed a novel and highly suggestive genome-wide association signal on Chr18 within a haplotype block containing the deleted in colorectal carcinoma (*Dcc*) and four other genes (*Stard6*, *4930503L19Rik*, *Poli*, *Mbd2*). We then used a reverse genetic approach to interrogate the role of *Dcc* in peripheral vestibular innervation. Although we acknowledge that the causal variant within the HMDP is as yet unidentified, the dose-dependent effects of *Dcc* deficiency seen in the knockout model support the association data and the utility of this approach.

METHODS

Animals and Genotyping

A detailed description of the HMDP (strain selection, statistical power, and mapping resolution) is provided by Bennett et al. (2010). Approximately four mice for each HMDP strain were purchased from the Jackson Laboratory (Bar Harbor, ME). There are no reported gender differences in vestibular function, so male and female mice were included. Mice were received at 4 weeks of age and aged to 6 weeks to ensure adequate acclimatization to a common environment ($n = 122$). HDMP strains were previously genotyped by the Broad Institute (Rau et al. 2015). Of the ~500,000 SNPs available, ~200,000 with allele frequencies ≥5 % were used for the association analysis. Conventional *Dcc* knockout mice on a 129Sv/C57BL6 mixed background were obtained from Dr. Marc Tessier-Lavigne (The Rockefeller University, NY) (Fazeli et al. 1997). Homozygous *Dcc* mutant mice have a perinatal lethal phenotype. Among offspring produced from heterozygous breeding pairs, 6-week-old $Dcc^{+/-}$ and wild-type (WT) control mice were used for VsEP analysis ($n = 11$ per group). For genotyping of *Dcc* knockout mice, polymerase chain reaction (PCR) was performed using the following three primers combined in a single reaction tube: DCCcode GGCCATTGAGGTTC CTTT, DCCrev AAGACGACCACACGCGAG, and NEO18.5 TCCTCGTGCTTTACGGTATC. The Institutional Care and Use Committee (IACUC) at the University of Southern California, Los Angeles, approved the animal protocol for the HMDP strains and the *Dcc* knockout mice (IACUC 12034). All analyses were performed by a researcher blinded to the genotype of the animals.

VsEP Equipment and Acquisition

VsEP recordings were based on methods detailed by Jones et al. (Jones et al. 2011). Mice from each strain were weighed and anesthetized with an intraperitoneal injection of ketamine (100 mg/kg bodyweight) and xylazine (10 mg/kg bodyweight) (n = 122, 11, and 11 for HMDP stains, $Dcc^{+/-}$, and WT mice, respectively). Recording electrodes were placed subcutaneously at the nuchal crest (noninverting electrode), behind the right pinna (inverting electrode), and at the base of the tail (ground electrode). A noninvasive spring clip was placed on the head and secured to a voltage-controlled mechanical shaker. Linear acceleration pulses lasting 2 ms each were applied to the cranium in the naso-occipital axis at a rate of 17 pulses per second. Pulses were presented using two polarities: normal (+Gx axis) and inverted (−Gx axis). Stimulus amplitudes ranged from +6 to −18 dB re: 1 g/ms (1.0 g = 9.8 m/s^2) and were presented in steps of 3 dB. VsEPs were recorded using traditional signal averaging. Electrophysiological activity was amplified (200,000×), filtered (300–3000 Hz), and digitized (125,000 Hz) beginning at stimulus onset. Responses ($n = 256$) were averaged to produce one response trace and replicated to provide at least two sets of waveform averages at each stimulus intensity. Waveforms were collected with and without the presence of broadband forward masker (50–50,000 Hz, 90 dB SPL). VsEP intensity series was collected beginning at the lowest stimulus intensity (−18 dB re: 1.0 g/ms) with and without acoustic masking, then in ascending 3 dB steps to +6 dB re: 1.0 g/ms.

VsEP Waveform Analysis

An observer blinded to the genotype of the animals analyzed VsEP thresholds. The first two positive and negative response peaks were analyzed. Peak latencies were measured in milliseconds from the onset of the stimulus to each positive and negative response peak. Peak-to-peak amplitudes were measured in microvolts from each positive response peak (P1 or P2) to the respective negative response peak (N1 or N2). Threshold (measured in dB re: 1.0 g/ms) was defined as the stimulus level midway between the jerk amplitude producing a discernible response and the stimulus level which did not. ABR Peak Analysis Software Version 0.9.0.2 ©Copyright 2007 Speech and Hearing Bioscience and Technology was used to analyze VsEP waveforms. Student's t test was performed for comparison of *Dcc* knockout mice and littermates. Cutoff for significance was set at $p = 0.05$. Elevated thresholds suggest reduced neural sensitivity, neural deficit, or reduced density of hair cell synaptic elements in the macular neuroepithelium.

Association Analysis

GWAS analyses for vestibular phenotypes in the HMDP strains were performed using genotypes of ~500,000 SNPs obtained from the Mouse Diversity Array (Yang et al. 2009). SNPs were required to have minor allele frequencies >5 % and missing genotype frequencies <10 %. Applying these filtering criteria resulted in a final set of 200,000 SNPs that were used for analysis. Association testing was performed using FaST-LMM (Lippert et al. 2011), a linear mixed model method that is fast and accounts for potential cofounding variables like population structure. To improve power, when testing all SNPs on a specific chromosome, the kinship matrix was constructed using the SNPs from all other chromosomes. The kinship matrix defines pairwise genetic relatedness among individuals and is usually estimated by using all

genotyped markers (Sul and Eskin 2013). This procedure includes the SNP being tested for association in the regression equation only once. Genome-wide significance threshold in the HMDP was determined by the family-wise error rate (FWER) as the probability of observing one or more false positives across all SNPs per phenotype. We ran 100 different sets of permutation tests and parametric bootstrapping of size 1000 and observed that the genome-wide significance threshold at a FWER of 0.05 corresponded to $p = 4.1 \times 10^6$, similar to what has been used in previous studies with the HMDP (Ghazalpour et al. 2012). This is approximately an order of magnitude larger than the threshold obtained by Bonferroni correction (4.6×10^7), which would be an overly conservative estimate of significance because nearby SNPs among inbred mouse strains are highly correlated with each other. Nonsynonymous SNPs within each region were downloaded from the Mouse Phenome Database (http://phenome.jax.org/). To check the validity of the GWAS association between variations at rs29632020 and the VsEP threshold metric, HMDP strains were separated into two groups based upon on genotype at rs29632020 (A/C). The mean VsEP threshold of each genotype group was used for statistical analysis.

Real-Time PCR

Six-week-old $Dcc^{+/-}$ and WT mice (n = 3 per group) and WT mice at P0 (n = 4) were euthanized, and bilateral inner ears were harvested. Vestibular ganglion and vestibular tissue were microdissected from the inner ear, left and right ear samples were combined, and immediately processed with RNAqueous® Total RNA Isolation Kit (Life Technologies) according to manufacturer's instructions. Total RNA was then converted to cDNA using the SuperScript® III First-Strand Synthesis SuperMix (Life Technologies). PCR was performed using the primer pairs acquired from applied biosystems: assay ID: Mm00514509_m1. Each sample was run in triplicate along with the housekeeping gene, *GAPDH*. Relative quantity of the transcript was determined using the $2^{-\Delta\Delta Ct}$ method using *GAPDH* as a reference (Schmittgen and Livak 2008).

In Situ Hybridization

In situ hybridization was performed as previously described (Ohyama et al. 2010). Briefly, embryonic day E15.5 heads were fixed in 4 % paraformaldehyde in PBS overnight at 4 °C, sunk in 30 % sucrose in PBS at 4 °C, incubated in Tissue-Tek O.C.T. compound (Sakura Finetek) at room temperature for 10 min, and frozen on dry ice. Sections, 14 µm thick, were cut using a Leica 3050 S cryostat. RNA probes for mouse *Dcc* (gifted by Dr. Roman Wunderlich, Institute for Cell and Neurobiology, Center for Anatomy, Charité-Universitätsmedizin Berlin, Germany) were synthesized, labeled with digoxigenin, and hydrolyzed by standard procedures. In situ hybridization images were obtained under bright-field microscopy (BZ9000; Keyence, Osaka, Japan).

Vestibular Immunostaining

Vestibular Whole-Mount Sample Preparation

Mouse vestibular tissues were dissected at desired time points and fixed with 4 % PFA for 20 min. Fixed samples were permeabilized with 0.5 % Trion X-100 followed by incubation in 10 % serum blocking buffer for 2 h at room temperature.

Vestibular Frozen Section Sample Preparation

Fixed heads were sequentially dehydrated in 15 and 30 % sucrose at 4 °C for approximately 12 h each step, embedded in Tissue-Tek O.C.T. compound (Sakura Finetek) and snap frozen on dry ice. Blocks were sectioned on a Leica 3050 S cryostat in a cranial-to-caudal direction using consecutive 12-µm sections starting at the superior semicircular canal proceeding to the most caudal section containing the cochlea.

Primary antibody incubation overnight at 4 °C was followed by secondary antibody incubation for 2 h at room temperature. Antibodies used in this study were as follows: goat anti-Dcc (1:100, Santa Cruz), Alexa 488-conjugated mouse anti-Tuj1 (1:300; Covance), mouse anti-CtBP2 (1:200 BD Biosciences), Alexa 594 donkey anti-rabbit (1:500, Life Technologies), Alexa Fluor-488 anti-mouse (1:50, Life Technologies), and Alexa Flour 594 rabbit anti-goat (1:500, Thermo Fisher). *Dcc* blocking peptide (1:50, Santa Cruz, sc-6535 P) was used for 3 h at RT as a control for the *Dcc* immunostaining experiments. Fluorescent dye Hoechst 33342 (0.1 µg/mL, SouthernBiotech) was used for DNA labeling. Confocal z-stack images were obtained using a laser confocal microscope (Olympus IX81) with epifluorescence light (Olympus Fluoview FV1000).

For neuronal cell body counts, tissue sections (n = 6 per group) were selected based on the presence of the following anatomical landmarks to ensure that the level of cut used for counting was similar across different mice: for superior vestibular ganglion cell counts, only sections with combined utricle and lateral crista in the same section were compared. For the inferior vestibular ganglion cell counts, only sections with combined saccule and facial nerve at its origin at the brainstem present in

the same slice were compared. For each ganglion, cell bodies were counted in two to three random 250-μm^2 regions and averaged. CtBP2 puncta were counted in 100-μm^2 areas containing five to six hair cells for adult utricle (6-week-old) and five to six hair cells at P0 (n = 4 per group). The Student's t test was used to compare means.

Statistical Analysis

Statistical analysis for VsEP, synaptic ribbon counts, and vestibular ganglion cell counts were performed using the Student's t test. GraphPad Prism 7 software was used to perform the tests. Continuous variables with normal distribution were expressed as mean ± standard deviation (SD). A two-tailed p value less than 0.05 indicated statistically significant differences.

RESULTS

Phenotypic Characterization of Vestibular Function in HMDP Mice Reveals Strain-Dependent Variation of VsEP Measures

To identify genomic regions associated with vestibular function, we first phenotyped the vestibular function of 6-week-old mice (n = 122) from 35 HMDP strains (n = 1–6/strain) using linear VsEPs. Linear VsEPs are compound action potentials from the vestibular portion of cranial nerve VIII and central relays in response to linear head jerk stimuli (Jones et al. 2006). The VsEP technique has been shown to selectively stimulate the utricle and saccule, also known as the otolith organs, as VsEP waveforms are undetectable in otoconia-deficient mice (Jones and Jones 1999). Similar to an auditory brainstem response (ABR), VsEP waveforms provide several quantifiable metrics of vestibular function (threshold, amplitude, and latency), each of which has been shown to represent a different aspect of vestibular afferent signaling (Jones and Jones 2014).

A wide range of VsEP thresholds were observed across the HMDP strains with a difference of 21 dB between the lowest and the highest strains (Fig. 1). BXD75/RwwJ, AXB13/PgnJ, AXB19a/PgnJ, and AXBB6/PgnJ strains equally showed the lowest level of VsEP threshold among 35 HMDP strains (−19.5 dB) whereas 129 × 1/SvJ exhibited the highest threshold (−1 dB). C57BL/6J (B6) showed a VsEP threshold of −9 dB. Similarly, VsEP P1N1 amplitude and P2 latency showed variation across strains. BXH19/TyJ and BXD84/RwwJ were strains with the lowest P1N1 amplitude (−2.75 and −2.7 dB, respectively), whereas AXB6/PgnJ and DBA/2J showed the highest level of P1N1 amplitude (1.2 and 1 dB, respectively) among 35 tested strains (data not shown).

VsEP Measurements Serve as a Valid Measure of Linear Accelerator Function for GWAS in Mice and Identify a Novel Candidate Gene

The factored spectrally transformed linear mixed models (FaST-LMM) is an algorithm for genome-wide association studies that has been shown to able to correct for several forms of confounding due to genetic relatedness in both mice and humans. This algorithm was applied to each VsEP metric (threshold, amplitude, latency) separately to identify genetic (SNP) associations. Adjusted association p values were calculated for ~200,000 SNPs with a minor allele frequency of >5 % (the $p < 0.05$ genome-wide equivalent for GWAS in the HMDP is $p = 4.1 \times 10^{-6}$, −log10P = 5.39). Association analysis using the threshold metric as a phenotype detected a highly suggestive association on Chr. 18 (peak SNP rs 29,632,020; $p = 4.58 \times 10^{-6}$) (Fig. 2A). Importantly, the minor allele frequency of rs29632020 was 40 %, indicating that the association signal was not simply due to a small number of outlier strains with extreme VsEP thresholds. In addition to this association, using VsEP amplitude as the phenotypic measure, we identified another highly suggestive association on Chr. 18 (peak SNP rs46114697; $p = 3.4 \times 10^{-5}$) (Fig. 2C, D). This peak SNP lies within a haplotype block containing only a few genes, one of which, *Slc12a2*, a Na-K-2Cl co-transporter, has been demonstrated to play a critical role in endolymphatic homeostasis in the otic vesicle and swim bladder of zebrafish, and mice carrying a mutation in this gene were deaf and demonstrated circling behavior indicative a vestibular functional deficit (Abbas and Whitfield 2009; Delpire et al. 1999).

Among the five genes (*Stard6*, *4930503L19Rik*, *Poli*, *Mbd2*, *Dcc*) at the Chr. 18 locus near peak SNP rs29632020, one gene, *Dcc*, has a well-established role in nervous system development (Fig. 2B). Using the publicly available expression data for several tissues in the HMDP (http://systems.genetics.ucla.edu), we were unable to identify a cis eQTL for *Dcc*. In addition to the eQTL analysis, we also used the Ensembl genome browser to see whether *Dcc* demonstrated amino acid substitutions among inbred strains that have been sequenced. One missense polymorphism in C57BL/6J was identified (Glu1237Lys) that is predicted to have functionally deleterious consequences by polyPhen and SIFT (score 0.1). The C57BL/6J genome is well represented in the 35 HMDP strains used in our GWAS, suggesting a potentially functional role for this missense mutation in the variation detected in the vestibular phenotype.

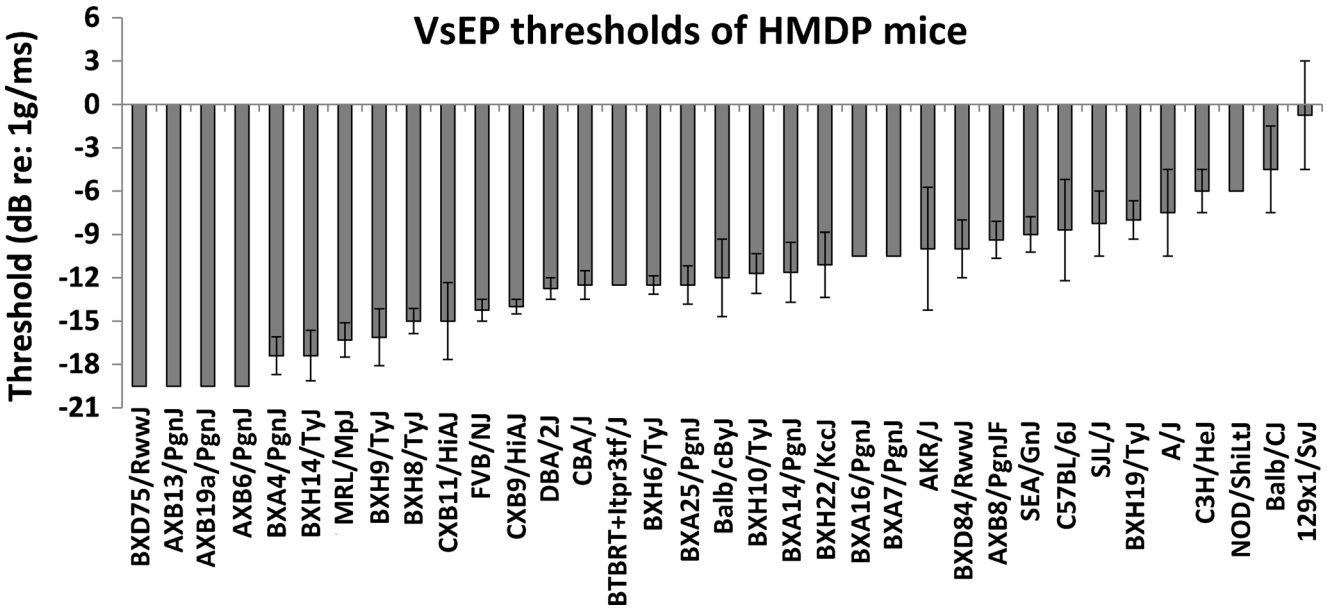

FIG. 1. VsEP characterization of HMDP mice reveals variation in afferent vestibular signaling among inbred strains. Mean ± standard error (SE) is shown for VsEP threshold.

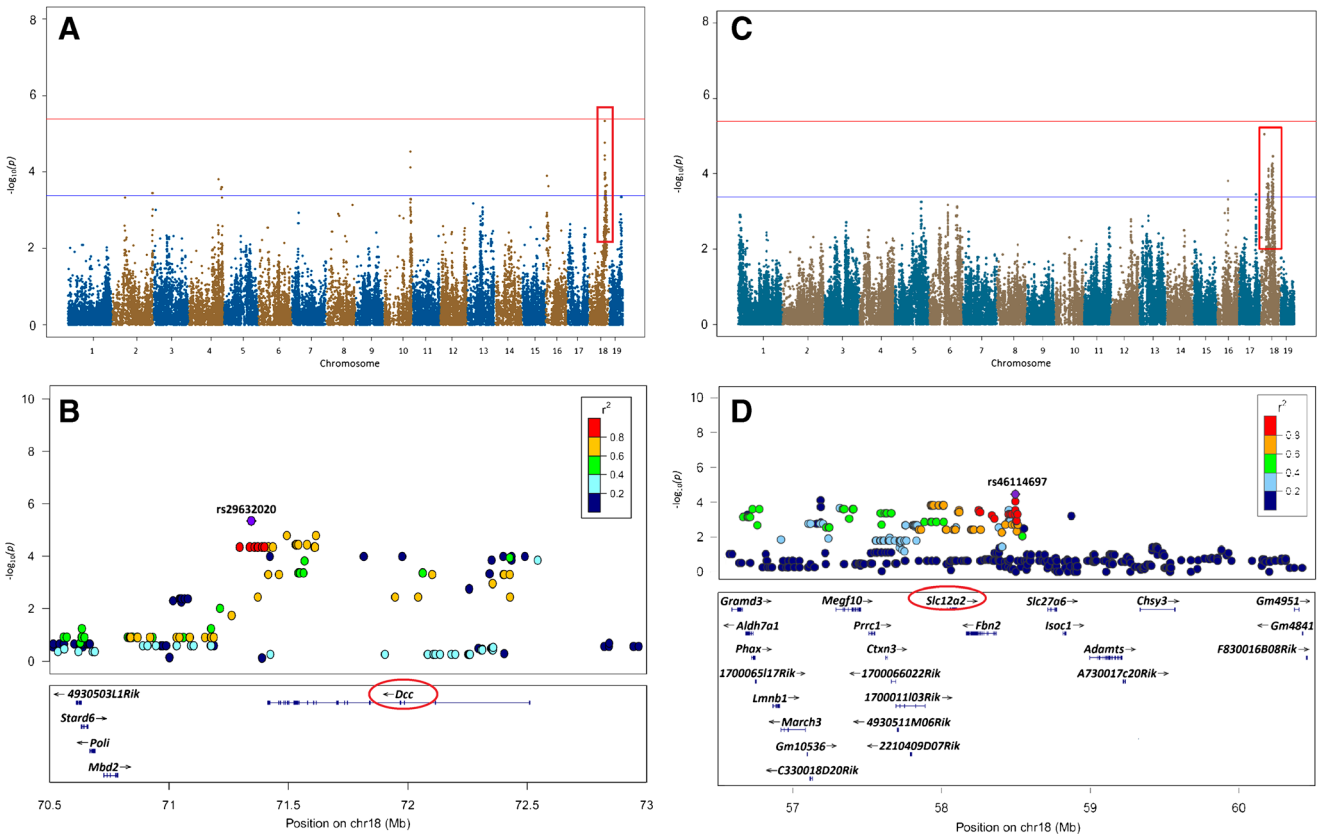

FIG. 2. GWAS results using 35 HMDP strains phenotyped with VsEPs. **A** Manhattan plot showing the association *p* values (−log10 transformed) as a function of SNP position in the genome. The analysis was performed using 189,613 SNPs with a minor allele frequency >5 %. Each chromosome is plotted on the *x*-axis in alternating *brown* and *blue colors*. SNP rs29632020 on Chr. 18 approached the predetermined genome-wide significance threshold when analyzing VsEP threshold (*red line*; −logP = 5.34). **B** Regional plot on Chr. 18 centered on the peak SNP rs29632020 (*purple diamond*; $p = 4.58E{-}06$). **C**, **D** Manhattan and regional plots, respectively, using VsEP amplitude as the trait. The regional plot shows *Slc12a2*, a Na-K-2Cl co-transporter known to play a critical role in endolymphatic homeostasis in the otic vesicle, in the association interval. The positions of all RefSeq genes are plotted using genome locations (NCBI's Build37 genome assembly). SNPs are colored based on their linkage disequilibrium (LD) with the peak SNP: *red* SNPs in LD at $r^2 > 0.8$, *orange* SNPs in LD at $r^2 > 0.6$, and *green* SNPs in LD at $r^2 > 0.4$.

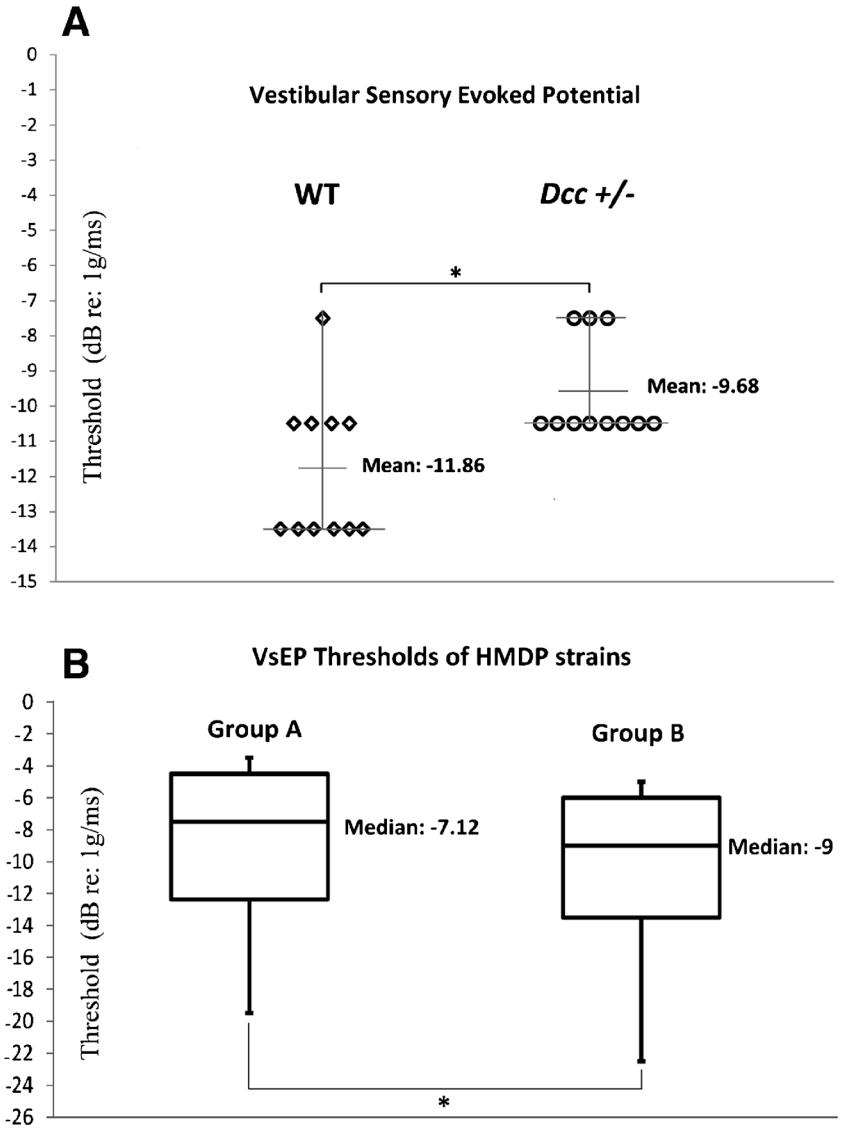

FIG. 3. Genetic variation in the *Dcc* affect VsEP threshold. Mice heterozygous for the *Dcc* knockout allele have elevated VsEP thresholds. Mean VsEP thresholds for 6-week-old $Dcc^{+/-}$ heterozygotes (−9.68 dB, SE = 0.42) showed statistically significant elevations in mean VsEP threshold relative to WT littermates (−11.86 dB, SE = 0.62) (*t* test $t(20) = 2.9$, $p = 0.013$, $n = 11$/group). **B** A statistically significant difference of −2.16 dB between the mean thresholds of group AA (mean −8.13 dB) and group CC (mean −10.29 dB) (*t* test $t(202) = 2.34$, $p = 0.019$) shows the variation of the strains for VsEP threshold as a function of genotype at peak SNP rs29632020. AA: AKR/J, BXH10/TyJ, BXH19/TyJ, BXH22/KccJ, BXH8/TyJ, C3H/HeJ, C57L/J, CBA/J, DBA/2J, NON/Ltj, NZW/LacJ, SEA/GnJ, SJL/J, SWR/J ($n = 70$). CC: A/J, AXB1/PgnJ, AXB13/PgnJ, m AXB15/PgnJ, AXB19a/PgnJ, AXB23/PgnJ, AXB6/PgnJ, AXB8/PgnJ, Balb/cByJ, Balb/cJ, BXA12/PgnJ, BXA13/PgnJ BXA14/PgnJ, BXA16/PgnJ, BXA25/PgnJ, BXA4/PgnJ, BXA7/PgnJ, BXD75/RwwJ, BXD84/RwwJ, BXH14/TyJ, BXH6/TyJ, BXH2/TyJ, BXH7/Tyj, BXH9/TyJ, C57BL/6J, CXB1/ByJ, CXB11/HiAJ, CXB2/ByJ, CXB9/HiAJ, FVB/NJ, LG/J, MRL/MpJ, NOR/LtJ, PL/J, RIIIS/J, NOD/ShiLtJ, BXH2/TyJ ($n = 185$).

Dcc is a cell surface receptor that binds the ligand Netrin-1, CBLN4, and possibly other still unknown signaling cues (Haddick et al. 2014). *Dcc* signaling plays an important role in carcinogenesis and in axonal migration (Krimpenfort et al. 2012; Mehlen et al. 2011). A previously published study demonstrated *Dcc* expression in the inner ear at E12.5 (Matilainen et al. 2007). Based on these data and the close proximity of our peak GWAS SNP (rs29632020) to *Dcc*, we focused on this candidate gene for its involvement in vestibular function.

Dcc-Deficient Mice ($Dcc^{+/-}$) Exhibit Defects in Afferent Vestibular Signaling

To directly test the hypothesis that *Dcc* is involved in vestibular function, we characterized previously generated *Dcc* knockout mice (Fazeli et al. 1997) using the

same VsEP technique. Mice that are homozygous for the *Dcc* knockout allele ($Dcc^{-/-}$) die within 24 h of birth due to severe neurological compromise (Fazeli et al. 1997). As the VsEP requires adult mice with mature vestibular systems, we performed the analysis on mice heterozygous for the mutant allele ($Dcc^{+/-}$). In support of our original GWAS finding, this analysis revealed a statistically significant elevation in VsEP threshold for $Dcc^{+/-}$ mice (–11.86 dB) compared to WT (–9.68 dB) littermates (*t* test $t(20) = 2.9$, $p = 0.013$; $n = 11$/group) (Fig. 3A). Furthermore, allelic variation at our peak SNP was statistically significantly associated with VsEP threshold in our HMDP (Fig. 3B). These data prompted us to look more closely at the vestibular system in $Dcc^{+/-}$ mice.

Dcc Expression in the Vestibular System of Prenatal and Adult Mice

In situ hybridization was performed to investigate *Dcc* mRNA expression in the vestibular tissues of E13.5 and E15.5 embryos, time points preceding the onset of innervation (Mbiene et al. 1988). This analysis showed that *Dcc* was expressed in the vestibular ganglion at E15.5 (Fig. 4A, B, D, E, H). Immunostaining of 6-week-old vestibular tissues revealed expression of Dcc protein in the sensory regions of the utricle and crista ampullaris (Fig. 5B, E). In the adult, *Dcc* expression was seen on neuronal cell bodies at the base of the utricle and on the projections of neurons to the crista ampullaris and utricle. This staining pattern is similar to that described in the neuronal cell bodies and projections in the optic tectum of *Xenopus* embryos and rat central nervous system (CNS) (Nagel et al. 2015; Keino-Masu et al. 1996; Horn et al. 2013). These findings suggested a potential role for *Dcc* in the process of innervation during development and potentially of maintenance of innervation into adulthood as seen in the mouse retinal ganglion and in CNS development (Mehlen and Mazelin 2003; Shi et al. 2010).

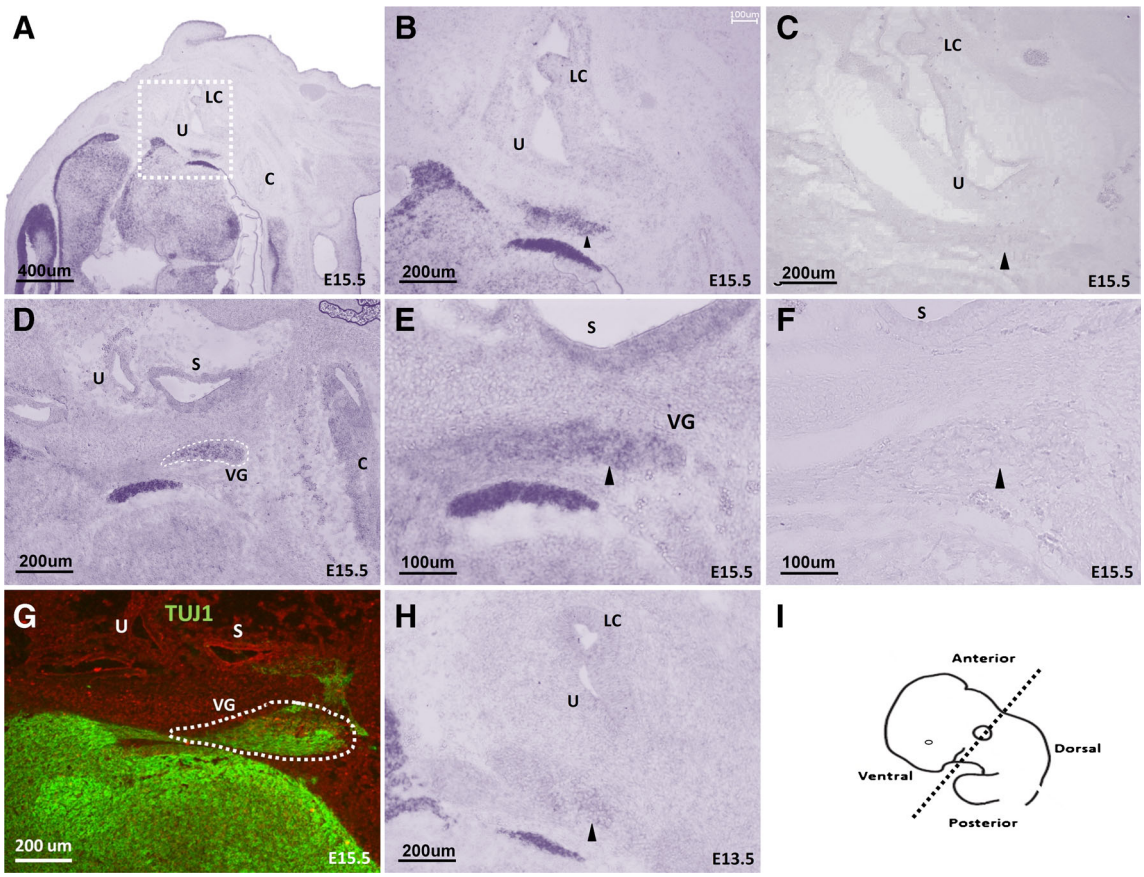

FIG. 4. *Dcc* is expressed in the developing vestibular system at E15.5. **A–C** In situ hybridization reveals expression of *Dcc* in the vestibular ganglia and vestibular epithelium. **G**, **H** *Dcc* expression and Tuj1 immunostaining of vestibular ganglia using adjacent frozen section blocks; Alexa Fluor-594 was used to show the background in *red*. **I** The plane of sections. *C* cochlea, *LC* lateral crista, *S* saccule, *U* utricle, *VG* vestibular ganglia.

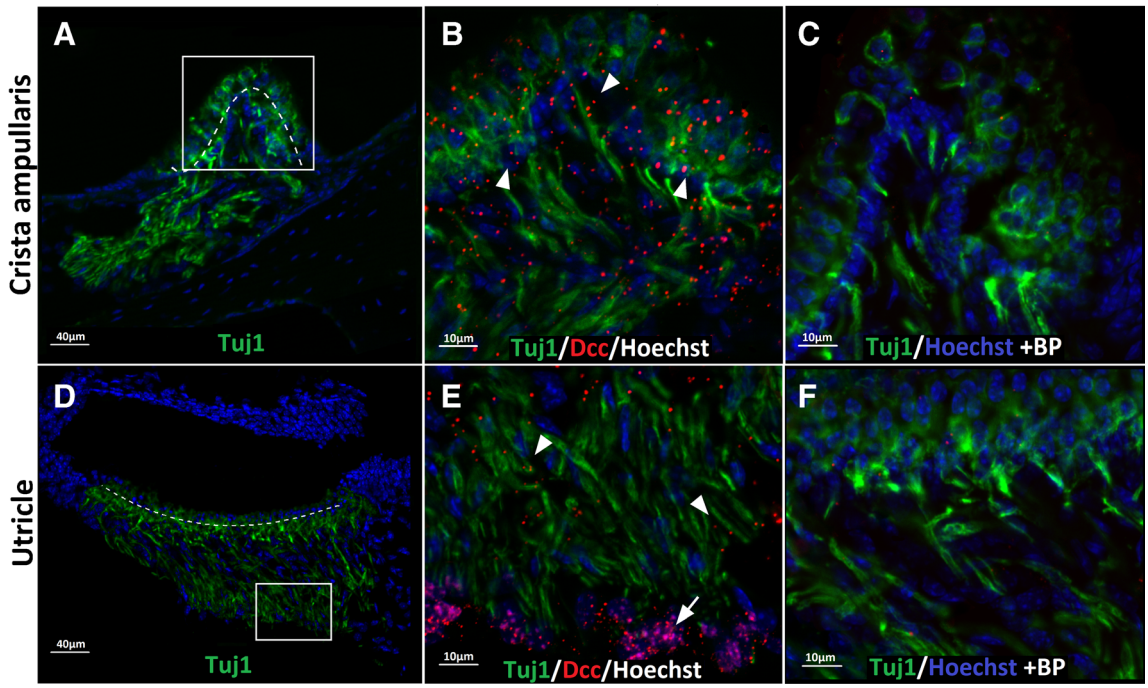

FIG. 5. *Dcc* expression in the vestibular tissues of adult mice. **A**, **D** Micrographs showing crista and utricle of WT mice (×20 magnification). *Boxes* outline areas of higher power images in **B**, **C**, **E**, and **F**. **B**, **E** *Dcc* detected in the crista ampullaris and utricle of 6-week-old mice. *Dcc* expression was seen on neuronal cell bodies at the base of the utricle (*arrow*) and on the projections of neurons to the crista ampullaris and utricle (*arrowheads*). **C**, **F** Crista ampullaris and utricle of adjacent sections were treated with *Dcc* blocking peptide. *Scale bar* 40 μm for **A** and **D**, and 10 μm for **B**, **C**, **E**, and **F**.

Dcc Heterozygotes Have Reduced Levels of *Dcc* in Vestibular Tissues and Support the Notion of a Dose-Dependent Effect

We next sought to verify reduced *Dcc* expression in the vestibular epithelium and ganglia of heterozygous mice to validate our hypothesis of a dose dependency to the phenotype. Real-time PCR showed 3.75-fold higher *Dcc* expression for WT mice (0.435) when compared to *Dcc* heterozygotes (0.116) (Fig. 5). Comparison of *Dcc* expression in WT mice at P0 and at 6-week-old showed 2.7-fold higher expression levels at P0 (0.89 and 0.33, respectively).

Dcc Is Required for Proper Synaptogenesis Between Utricle and Vestibular Nerve Afferent Fibers

As prior studies have demonstrated VsEP thresholds are inversely proportional to the density of hair cell synapses in the macular epithelium (Jones and Jones 2014), we hypothesized that the elevated VsEP thresholds observed in the $Dcc^{+/-}$ mice may arise from defects in innervation between the otolith organ hair cells and vestibular afferent neurons. We next analyzed synaptic density in utricles by immunolabeling the presynaptic marker of synaptic ribbon complexes (CtBP2); at postnatal day 0 (P0), $Dcc^{+/-}$ mice appeared to have fewer CtBP2 puncta than wild-type littermates, but this difference did not reach statistical significance (t test $t(6) = 1.68$, $p = 0.136$). In contrast, adult $Dcc^{+/-}$ mice (6-week-old) showed significantly lower CtBP2 counts compared to WT controls (t test $t(6) = 3.07$, $p = 0.02$), suggesting a role for *Dcc* in the maintenance of synapses in the aging utricle (Figs. 6 and 7B). There was a notable difference between WT and $Dcc^{-/-}$ (P0 mice), with approximately 1.8-fold difference in CtBP2 puncta (t test $t(6) = 7.36$, $p = 0.0002$). These findings suggest that *Dcc* plays a role in utricular innervation and does so in a dose-dependent manner (Fig. 7).

Dcc Deficiency Results in Reduced Vestibular Ganglion Cell Counts and Abnormal Innervation of the Vestibular Epithelia

Based on the findings thus far, we hypothesized that the defects in utricular synaptogenesis observed in *Dcc* deficient mice may reflect abnormal axonal path finding or a developmental and/or survival defect of vestibular neurons. To test this hypothesis, we analyzed axonal projections and vestibular ganglion cell counts in tissue sections of WT, $Dcc^{+/-}$, and $Dcc^{-/-}$ mice using antibodies for the neuronal marker beta-3-tubulin (TuJ1) and the Hoechst nucleic acid stain. At P0, vestibular ganglion cell counts of $Dcc^{-/-}$ mice

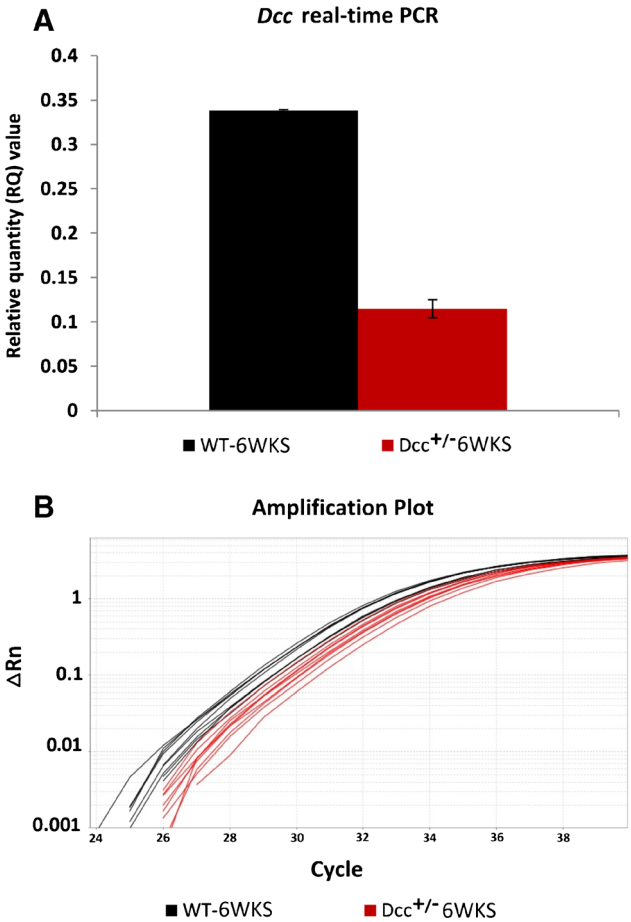

FIG. 6. Quantitative real-time PCR revealed 3.75-fold higher *Dcc* expression in adult (6-week-old) WT mice (0.435) as compared to adult *Dcc* heterozygotes (0.116). **B** The amplification plot for $Dcc^{+/-}$ and WT samples (n = 3 per group).

showed a statistically significant (SVG: t test $t(10) = 3.3$, $p = 007$; IVG: $t(10) = 3.2$, $p = 0.009$) reduction in the numbers of cell bodies when compared to WT controls (Fig. 7F, G, K). As shown in Fig. 8, whole-mount staining with TuJ1 at embryonic stages showed abnormal innervation patterns to the utricle, saccule, and semicircular canal crista (n = 3/group) at E14.5, E16.6, and E18.5. These findings suggest that *Dcc* plays a role in vestibular ganglion cell number at the time of determination/differentiation, delamination and developmental migration, and/or survival. $Dcc^{-/-}$ mice at P0 showed abnormal innervation of the vestibular hair cells. There were no detectable abnormalities of the utricular hair cells (Fig. 7H, I). The results of our qualitative assays investigating the axonal organization in adult $Dcc^{+/-}$ mice showed phenotypic variation. $Dcc^{+/-}$ mice in some instances showed axonal organization similar to WT mice (Fig. 6K, N). However, other $Dcc^{+/-}$ mice had reduced axonal density in the semicircular canal crista as compared to WT mice (Fig. 6L, O). We could not identify any differences in utriclar innervation patterns (sagittal cuts of utricle) between the $Dcc^{+/-}$ and WT mice (data not shown).

DISCUSSION

Beginning to Define the Genetics of Functional Variation in the Mouse Vestibular System Through GWAS

Understanding population variation in vestibular function at the molecular level is a critical step toward developing targeted therapies. Dizziness, particularly in the elderly, is common but not universal and likely results from the interplay between environmental and genetic susceptibilities. Very little is known about the genetics of vestibular function within populations. In an effort to circumvent the limitations of human studies, mouse GWAS has revolutionized the field of genetics and has led to the discovery of genes that are involved in complex traits often with translation to human disease (Civelek and Lusis 2014). In this study, we have added to the literature on strain variation in VsEP measurements by characterizing 35 inbred mouse strains validating this metric for genome-wide studies and have, for the first time, used association analysis with correction for population structure to map loci for vestibular functional variation in inbred strains of mice. Our results identify two suggestive loci for strain variation in VsEPs, a quantitative measure of linear accelerator function.

Our successful mapping largely came from the initial observation that there was clear strain variation in VsEP phenotypes, reiterating the contribution of genetic factors to vestibular function. We measured VsEPs in a portion of the HMDP with 35 classical inbred and recombinant inbred mouse strains for association mapping. Previous studies using the HMDP demonstrated that the panel provided sufficient statistical power and resolution to identify a novel locus that was modeled in a mutant strain (Ghazalpour et al. 2012). Although this panel is composed of over 100 commercially available inbred strains, with roughly one third of this panel, we were able to map a locus with high resolution. The resolution of this panel is, in some cases, two orders of magnitude greater than that achieved with linkage analysis, as we have recently demonstrated in our mouse GWAS for age-related hearing loss and noise-induced hearing loss (Lavinsky et al. 2015; Ohmen et al. 2014). Genetic approaches in humans and mice (such as linkage analysis and GWAS) can identify candidate variants but are often insufficiently powered to specifically identify causal variants. Locus heterogeneity for both Mendelian and complex traits contributes to this difficulty and likely represents

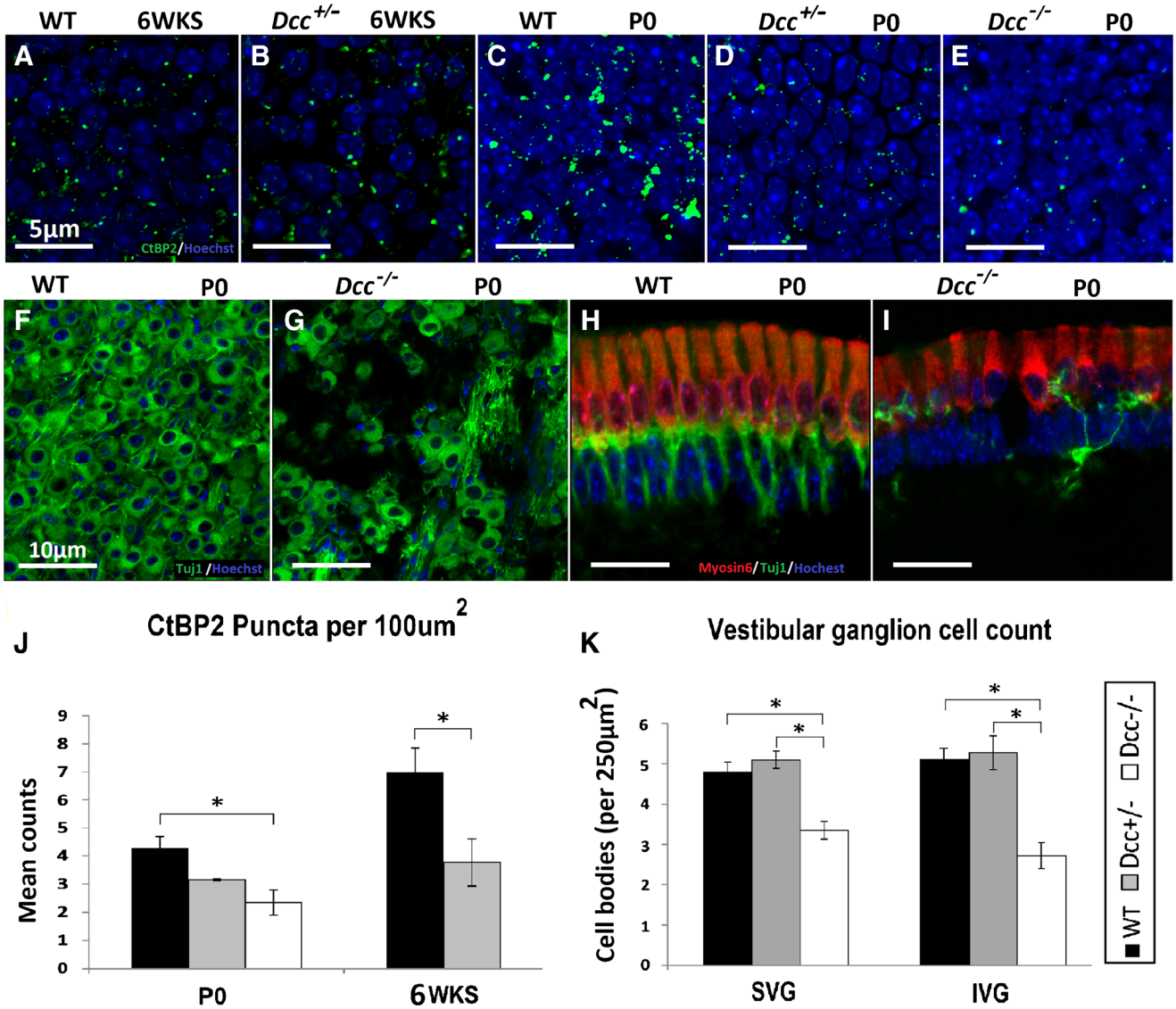

FIG. 7. Dose-dependent effect of *Dcc* on utricular synapse formation. **A–E** Utricles from $Dcc^{-/-}$, $Dcc^{+/-}$, and WT mice immunostained for the presynaptic marker CtBP2 show a progressive decrease in CtBP2 puncta. *Scale bar* = 5 µm. **F**, **G** Micrographs representatives of the vestibular ganglion cells of the WT and $Dcc^{-/-}$ mice show missing cells in *Dcc* knockouts (n = 3 per group). **H**, **I** Micrographs show abnormal utricular hair cells innervation of $Dcc^{-/-}$ as compared to WT controls (n = 3 per group). **B** Quantification of mean CtBP2 foci from $Dcc^{-/-}$, $Dcc^{+/-}$, and WT mice at P0 and 6 weeks of age (n = 4 per group) per 100-µm^2 area. *$p < 0.05$. Error bars ± 1 SE. **C** Vestibular ganglion cell count at P0. Superior (SVG) and inferior vestibular ganglia (IVG) cell counts revealed a statistically significant decrease for $Dcc^{-/-}$ mice in comparison to $Dcc^{+/-}$, and WT mice (n = 6 per group). There was no statistically significant difference in mean cell body count of the $Dcc^{+/-}$ and WT mice. *$p < 0.05$. Error bars ± 1 SE.

some of the "missing heritability" for many common diseases (Berndt et al. 2011; Ghoussaini et al. 2012; Hein et al., 2012; Sanna et al. 2011). An additional barrier to causal SNP identification in mouse genetic studies is the large haplotype blocks that exist within the mouse genome in comparison to humans (Guryev et al. 2006). In the present study, we applied this new paradigm to the first high-resolution mapping of candidate genes for vestibular functional variation. Our GWAS generated an association peak SNP on mouse chromosome 18 lying in close proximity to the gene *Dcc*. Variation in the peak SNP was statistically significantly associated with variation in VsEP threshold when looking at the extremes of this metric within the HMDP. All of the RI strains within the HMDP are derived from C57BL/6J and Ensembl predicted a single missense allele (Glu1237Lys) within *Dcc* in this strain to be deleterious. Interestingly and in support of this finding, as seen in Fig. 2, C57BL/6J lies to the right on the continuum of elevated VsEP threshold. Unfortunately, the Glu1237Lys variant present in C57BL/6J was not used in our GWAS so an effect

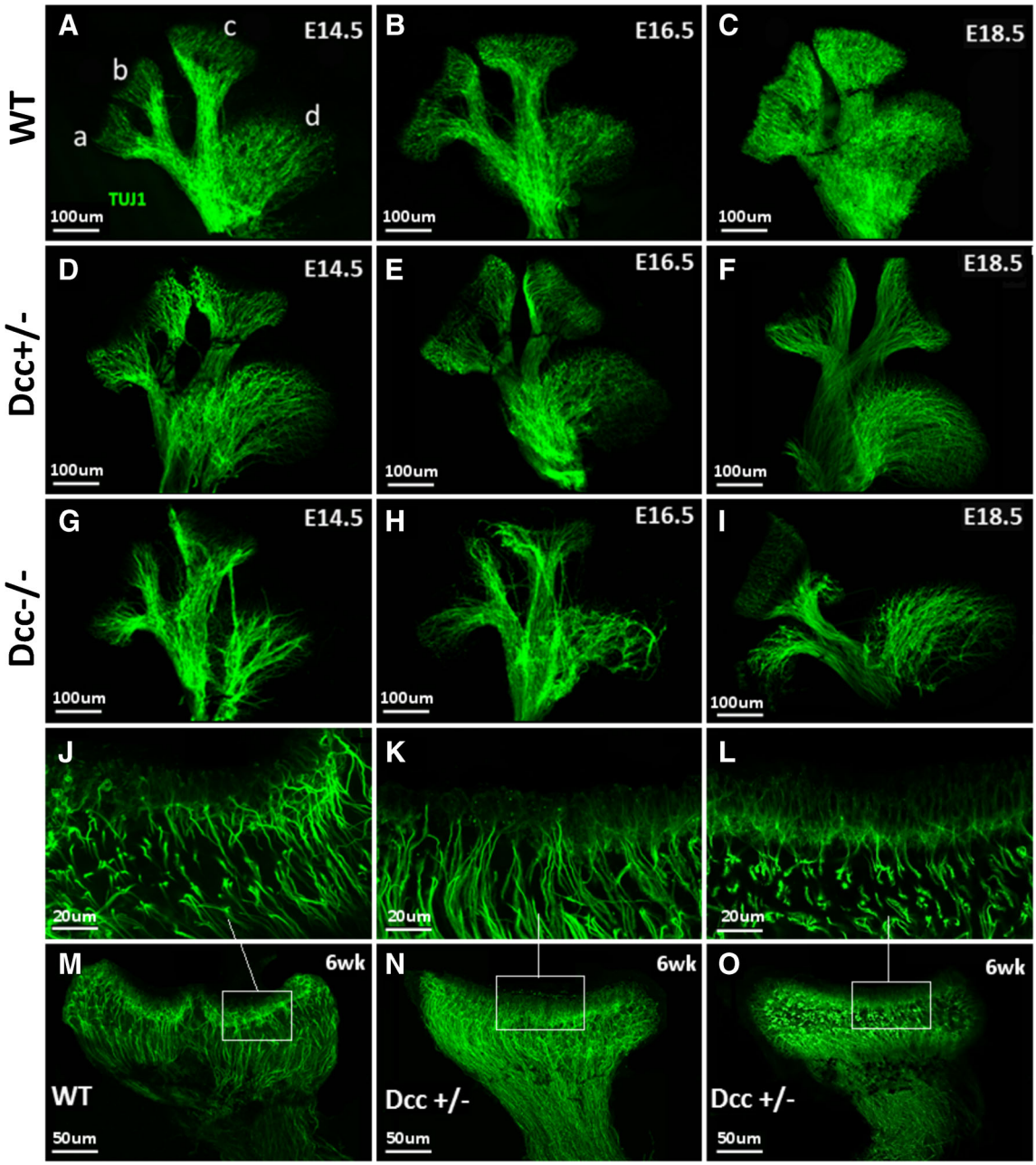

FIG. 8. **A–I** Whole-mount TuJ1-stained utricle and crista from $Dcc^{-/-}$, $Dcc^{+/-}$and WT embryos. Morphological changes of $Dcc^{-/-}$ mutants are shown as disorganized axons or absence of axons of the utricle and crista at E14.5, E16.6, and E18.5 (n = 3/group). *Scale bar* 200 μm. **J–O** Whole-mount TuJ1-stained crista with two phenotypic variation for $Dcc^{+/-}$ mutants. $Dcc^{+/-}$ mice in some instances showed axonal organization similar to WT mice (**K**, **N**). The other $Dcc^{+/-}$ mice had reduced axonal density in comparison to WT mice (**L**, **O**). For consistency, ~22 confocal optical sections, spanning a tissue thickness of ~16 μm, were collected for each sample (n = 4/group). **G**, **H** Frozen sections (sagittal cut) of utricle stained with TuJ1 and Hoechst 33342 did not show any identifiable difference in neuron projection pattern between the $Dcc^{+/-}$ and WT mice (n = 4/group). *Scale bar* 40 μm for **A–C**, **G**, and **H**. *Scale bar* 100 μm for **D–F**.

could not be ascertained directly; however, the proximity of this coding SNP (rs29561610; 71,465,755 bp) to our peak SNP (rs29632020; 71,344,563 bp) could place it within the associated haplotype block and warrants further investigation. A natural next step, however, was to consider the impact of *Dcc* deficiency in a mouse with a targeted deletion.

Dcc Is Expressed in Prenatal and Postnatal Vestibular Neurons

Expression analysis in the embryonic vestibular tissues revealed robust expression in the vestibular ganglion at E15.5, a critical time of neuronal maturation but preceding innervation of the vestibular sensory epi-

thelia. The result of the immunostaining of the utricle and crista in 6-week-old mice showed that *Dcc* expression continues into adulthood in the neurons innervating the utricle and crista ampullaris. These data support the notion that *Dcc* plays a critical role in the developmental processes of innervation of the vestibular sensory organs and potentially in the maintenance of innervation into adulthood consistent with our finding of reduced synaptic ribbon density in 6-week-old *Dcc*-deficient mice in comparison to P0. Confirmation of the latter hypothesis will require a longitudinal analysis of *Dcc*-deficient mice as they age.

Dcc Plays a Role in Normal Vestibular Innervation

Linear acceleration is transformed into neural signals by macular hair cells of the utricle and saccule. These hair cells synapse with primary sensory neurons that then communicate with secondary neurons in the brainstem vestibular nuclei. In this manuscript, we have demonstrated, through a forward genetics approach, that *Dcc* plays a role in the afferent signaling of the utricle through the in-depth characterization of a *Dcc* knockout strain, and that it does so by influencing vestibular ganglion cell counts, axonal projection, and synaptic density.

Our preliminary GWAS data implicating *Dcc* in vestibular functional variation supported our hypothesis that *Dcc* deficiency leads to defects in vestibular ganglion axon formation and in vestibular synaptogenesis. We subsequently pursued an in-depth analysis of this process in *Dcc* constitutive knockout mice.

Dcc-deficient mice have a dose-dependent defect in vestibular sensory epithelial innervation and synaptogenesis. The variable expression of the phenotype noted during our investigation is the likely result of the mixed background of the knockout model and suggests the existence of modifier genes within the parental strains. The mechanisms underlying the reduced ganglion cell counts could be developmental, occurring at the time of neural determination and/or delamination and/or acquired due to premature cell death. Similarly, the mechanism underlying the aberrant innervation remains unknown and will require the generation of spatially and temporally specific *Dcc* knockout strains.

CONCLUSIONS

In this manuscript, we have, for the first time, used association analysis with correction for population structure to map loci for vestibular functional variation in inbred strains of mice. Our results add to the literature on strain variation in VsEP metrics, support the notion of a genetic component to vestibular function, and identify a novel gene responsible strain variation in vestibular sensory-evoked potentials, a quantitative measure of linear accelerator function. Our findings validate the power of the HMDP for detecting genes involved in vestibular functional variation and shed new light on a molecular pathway that is necessary for normal innervation of the mouse vestibular system. Future studies will likely include tissue-specific knockout of *Dcc* and *Netrin-1* in the inner ear using a Cre/Lox system and will help to delineate the developmental basis for the vestibular defects seen in *Dcc*-deficient mice.

ACKNOWLEDGMENTS

This research is supported by the National Institutes of Health (NIH) grants R01 DC010856-01 (RAF) and HL28481 (AJL). The authors would like to thank Dr. Neil Segil, Dr. Sherri Jones, Dr. Bernd Fritzsch, and Dr. Radha Kalluri for thoughtful discussion and advice. We would also like to thank Litao Tao, Juan Llamas, Toru Miwa, Mete Civelek, Calvin Pan, Maria Gómez-Casati, Sarath Vijayakumar, Christopher Ventura, Nicole Grepo, and Olav Olsen for technical advice. We would like to thank Roman Wunderlich for providing the *Dcc* in situ probe and Dr. Marc Tessier-Lavigne for providing the *Dcc* knock-out mice.

Contribution of Authors R.A.F., J.L., T.O., and A.J.L. designed and supervised the experiments. P.S performed VsEP for $Dcc^{+/-}$, CTBP2 count for adult mice, immunostaining of VG, prepared images for in situ hybridization, *Dcc* expression in adult mice, qPCR, Fig. 8D–F, I–O, organized all figures and tables, and completed manuscript writing. A.M. performed VG cell count, P0 CTBP2 count, validated the variation of the HMDP strains for VsEP, and participated in manuscript writing. Y.J.K. and L.I.Z. designed vestibular system neuron projection pattern at embryonic stage and prepared Fig. 8A–C, G, H. Manhattan and regional plots were prepared by A.M.C., J.H., E.E, and H.A following FaST-LMM. M.K.H. set up the VsEP device and VsEP protocol. J.L. performed and analyzed VsEP for HMDP strains. C.C and T.O. preformed in situ hybridization. M.G. contributed in genotyping and confocal imaging.

REFERENCES

Abbas L, Whitfield TT (2009) Nkcc1 (Slc12a2) is required for the regulation of endolymph volume in the otic vesicle and swim bladder volume in the zebrafish larva. Development 136:2837–2848

Bennett BJ, Farber CR, Orozco L, Kang HM, Ghazalpour A, Siemers N, Neubauer M, Neuhaus I, Yordanova R, Guan B, et al. (2010) A high-resolution association mapping panel for the dissection of complex traits in mice. Genome Res 20:281–290

BERNDT SI, SAMPSON J, YEAGER M, ET AL. (2011) Large-scale fine mapping of the HNF1B locus and prostate cancer risk. Hum Mol Genet 16:3322–3329

BUSH WS, MOORE JH (2012) Chapter 11: Genome-wide association studies. PLoS Comput Biol 8:e1002822

CIVELEK M, LUSIS AJ (2014) Systems genetics approaches to understand complex traits. Nat Rev Genet 15:34–48

DAVIS RC, VAN NAS A, BENNETT B, OROZCO L, PAN C, RAU CD, ESKIN E, LUSIS AJ (2013) Genome-wide association mapping of blood cell traits in mice. Mamm Genome 24:105–118

DELPIRE E, LU J, ENGLAND R, DULL C, THORNE T (1999) Deafness and imbalance associated with inactivation of the secretory Na-K-2Cl co-transporter. Nat Genet 22:192–195

EPPSTEINER RW, SMITH RJ (2011) Genetic disorders of the vestibular system. Curr Opin Otolaryngol Head Neck Surg 19:397–402

FARBER CR, BENNETT BJ, OROZCO L, ZOU W, LIRA A, KOSTEM E, KANG HM, FURLOTTE N, BERBERYAN A, GHAZALPOUR A, ET AL. (2011) Mouse genome-wide association and systems genetics identify Asxl2 as a regulator of bone mineral density and osteoclastogenesis. PLoS Genet 7:e1002038

FAZELI A, DICKINSON SL, HERMISTON ML, TIGHE RV, STEEN RG, SMALL CG, STOECKLI ET, KEINO-MASU K, MASU M, RAYBURN H, ET AL. (1997) Phenotype of mice lacking functional Deleted in colorectal cancer (Dcc) gene. Nature 386:796–804

GHAZALPOUR A, RAU CD, FARBER CR, BENNETT BJ, OROZCO LD, VAN NAS A, PAN C, ALLAYEE H, BEAVEN SW, CIVELEK M, ET AL. (2012) Hybrid mouse diversity panel: a panel of inbred mouse strains suitable for analysis of complex genetic traits. Mamm Genome 23:680–692

GOODYEAR RJ, JONES SM, SHARIFI L, FORGE A, RICHARDSON GP (2012) Hair bundle defects and loss of function in the vestibular end organs of mice lacking the receptor-like inositol lipid phosphatase PTPRQ. J Neurosci 32:2762–2772

GHOUSSAINI M, FLETCHER O, MICHAILIDOU K, ET AL. (2012) Genome-wide association analysis identifies three new breast cancer susceptibility loci. Nat Genet 3:312–318

GURYEV V, KOUDIJS MJ, ET AL. (2006) Genetic variation in the zebrafish. Genome Res 4:491–497

HADDICK PC, TOM I, LUIS E, QUINONES G, WRANIK BJ, RAMANI SR, STEPHAN JP, TESSIER-LAVIGNE M, GONZALEZ LC (2014) Defining the ligand specificity of the deleted in colorectal cancer (DCC) receptor. PLoS One 9:e84823

HEIN R, MARANIAN M, HOPPER JL, ET AL. (2012) COMPARISON OF 6Q25 BREAST CANCER HITS FROM ASIAN AND EUROPEAN GENOME WIDE ASSOCIATION STUDIES IN THE BREAST CANCER ASSOCIATION CONSORTIUM (BCAC). PLOS ONE 8,E42380

HORN KE, GLASGOW SD, GOBERT D, ET AL. (2013) DCC expression by neurons regulates synaptic plasticity in the adult brain. Cell Rep 1:173–185

HUANG L, KUO YM, GITSCHIER J (1999) The pallid gene encodes a novel, syntaxin 13-interacting protein involved in platelet storage pool deficiency. Nat Genet 23:329–332

HUI ST, PARKS BW, ORG E, NORHEIM F, CHE N, PAN C, CASTELLANI LW, CHARUGUNDLA S, DIRKS DL, PSYCHOGIOS N, ET AL. (2015) The genetic architecture of NAFLD among inbred strains of mice. Elife 4:e05607

HURLE B, IGNATOVA E, MASSIRONI SM, MASHIMO T, RIOS X, THALMANN I, THALMANN R, ORNITZ DM (2003) Non-syndromic vestibular disorder with otoconial agenesis in tilted/mergulhador mice caused by mutations in otopetrin 1. Hum Mol Genet 12:777–789ISOSOMPPI J, VASTINSALO H, GELLER SF, HEON E, FLANNERY JG, SANKILA EM (2009) Disease-causing mutations in the CLRN1 gene alter normal CLRN1 protein trafficking to the plasma membrane. Mol Vis 15:1806–1818

JEN JC (2008) Recent advances in the genetics of recurrent vertigo and vestibulopathy. Curr Opin Neurol 21:3–7

JONES SM, JOHNSON KR, YU H, ERWAY LC, ALAGRAMAM KN, POLLAK N, JONES TA (2005) A quantitative survey of gravity receptor function in mutant mouse strains. JARO 6:297–310

JONES SM, JONES TA (2014) Genetics of peripheral vestibular dysfunction: lessons from mutant mouse strains. J Am Acad Audiol 25:289–301

JONES SM, JONES TA, JOHNSON KR, YU H, ERWAY LC, ZHENG QY (2006) A comparison of vestibular and auditory phenotypes in inbred mouse strains. Brain Res 1091:40–46

JONES SM, ROBERTSON NG, GIVEN S, GIERSCH AB, LIBERMAN MC, MORTON CC (2011) Hearing and vestibular deficits in the Coch(−/−) null mouse model: comparison to the Coch (G88E/G88E) mouse and to DFNA9 hearing and balance disorder. Hear Res 272:42–48

JONES TA, JONES SM (1999) Short latency compound action potentials from mammalian gravity receptor organs. Hear Res 136:75–85

KEINO-MASU K, MASU M, HINCK L, LEONARDO ED, CHAN SS, CULOTTI JG, TESSIER-LAVIGNE M (1996) Deleted in colorectal cancer (DCC) encodes a netrin receptor. Cell 2:175–185

KERBER KA, MEURER WJ, WEST BT, FENDRICK AM (2008) Dizziness presentations in U.S. emergency departments, 1995-2004. Acad Emerg Med 15:744–750

KRIMPENFORT P, SONG JY, PROOST N, ZEVENHOVEN J, JONKERS J, BERNS A (2012) Deleted in colorectal carcinoma suppresses metastasis in p53-deficient mammary tumours. Nature 482:538–541

LAVINSKY J, CROW AL, PAN C, WANG J, AARON KA, HO MK, LI Q, SALEHIDE P, MYINT A, MONGES-HERNADEZ M, ET AL. (2015) Genome-wide association study identifies nox3 as a critical gene for susceptibility to noise-induced hearing loss. PLoS Genet 11:e1005094

LEE SI, CONRAD T, JONES SM, LAGZIEL A, STAROST MF, BELYANTSEVA IA, FRIEDMAN TB, MORELL RJ (2013) A null mutation of mouse Kcna10 causes significant vestibular and mild hearing dysfunction. Hear Res 300:1–9

LIPPERT C, LISTGARTEN J, LIU Y, KADIE CM, DAVIDSON RI, HECKERMAN D (2011) FaST linear mixed models for genome-wide association studies. Nat Methods 8:833–835

MATILAINEN T, HAUGAS M, KREIDBERG JA, SALMINEN M (2007) Analysis of Netrin 1 receptors during inner ear development. Int J Dev Biol 51:409–413

MBIENE JP, FAVRE D, SANS A (1988) Early innervation and differentiation of hair cells in the vestibular epithelia of mouse embryos: SEM and TEM study. Anat Embryol 4:331–340

MEHLEN P, MAZELIN L (2003) The dependence receptors DCC and UNC5H as a link between neuronal guidance and survival. Biol Cell 7:425–436

MEHLEN P, DELLOYE-BOURGEOIS C, CHEDOTAL A (2011) Novel roles for Slits and netrins: axon guidance cues as anticancer targets? Nat Rev Cancer 11:188–197

NAKANO Y, LONGO-GUESS CM, BERGSTROM DE, NAUSEEF WM, JONES SM, BANFI B (2008) Mutation of the Cyba gene encoding p22phox causes vestibular and immune defects in mice. J Clin Invest 118:1176–1185

NAGEL AN, MARSHAK S, MANITT C, SANTOS RA, PIERCY MA, MORTERO SD, SHIRKEY-SON NJ, COHEN-CORY S (2015) Netrin-1 directs dendritic growth and connectivity of vertebrate central neurons in vivo. Neural Dev. doi:10.1186/s13064-015-0041-y

NEUHAUSER HK, VON BREVERN M, RADTKE A, LEZIUS F, FELDMANN M, ZIESE T, LEMPERT T (2005) Epidemiology of vestibular vertigo: a neurotologic survey of the general population. Neurology 65:898–904

OHMEN J, KANG EY, LI X, JOO JW, HORMOZDIARI F, ZHENG QY, DAVIS RC, LUSIS AJ, ESKIN E, FRIEDMAN RA (2014) Genome-wide association study for age-related hearing loss (AHL) in the mouse: a meta-analysis. JARO 15:335–352

Ohyama T, Basch ML, Mishina Y, Lyons KM, Segil N, Groves AK (2010) BMP signaling is necessary for patterning the sensory and nonsensory regions of the developing mammalian cochlea. J Neurosci 30:15044–15051

Paffenholz R, Bergstrom RA, Pasutto F, Wabnitz P, Munroe RJ, Jagla W, Heinzmann U, Marquardt A, Bareiss A, Laufs J, et al. (2004) Vestibular defects in head-tilt mice result from mutations in Nox3, encoding an NADPH oxidase. Genes Dev 18:486–491

Park CC, Gale GD, de Jong S, Ghazalpour A, Bennett BJ, Farber CR, Langfelder P, Lin A, Khan AH, Eskin E, et al. (2011) Gene networks associated with conditional fear in mice identified using a systems genetics approach. BMC Syst Biol 5:43

Rau CD, Parks B, Wang Y, Eskin E, Simecek P, Churchill GA, Lusis AJ (2015) High-density genotypes of inbred mouse strains: improved power and precision of association mapping. G3 (Bethesda) 5:2021–2026

Sanna S, Li B, Mulas A, Sidore C, et al. (2011) Fine mapping of five loci associated with low-density lipoprotein cholesterol detects variants that double the explained heritability. PLoS Genet 7, e1002198

Schmittgen TD, Livak KJ (2008) Analyzing real-time PCR data by the comparative C(T) method. Nat Protoc 3:1101–1108

Shi M, Zheng MH, Liu ZR, ZL H, Huang Y, Chen JY, Zhao G, Han H, Ding YQ (2010) DCC is specifically required for the survival of retinal ganglion and displaced amacrine cells in the developing mouse retina. Dev Biol 1:87–96

Smolock EM, Ilyushkina IA, Ghazalpour A, Gerloff J, Murashev AN, Lusis AJ, Korshunov VA (2012) Genetic locus on mouse chromosome 7 controls elevated heart rate. Physiol Genomics 44:689–698

Sul JH, Eskin E (2013) Mixed models can correct for population structure for genomic regions under selection. Nat Rev Genet 4:300

Vincent PF, Bouleau Y, Safieddine S, Petit C, Dulon D (2014) Exocytotic machineries of vestibular type I and cochlear ribbon synapses display similar intrinsic otoferlin-dependent Ca2+ sensitivity but a different coupling to Ca2+ channels. J Neurosci 34:10853–10869

Yang H, Ding Y, Hutchins LN, Szatkiewicz J, Bell TA, Paigen BJ, Graber JH, de Villena FP, Churchill GA (2009) A customized and versatile high-density genotyping array for the mouse. Nat Methods 6:663–666

Zhou X, Crow AL, Hartiala J, Spindler TJ, Ghazalpour A, Barsky LW, Bennett BJ, Parks BW, Eskin E, Jain R, et al. (2015) The genetic landscape of hematopoietic stem cell frequency in mice. Stem Cell Rep 5:125–138